

Had You Looked Where I'm Looking: Cross-user Similarities in Viewing Behavior for 360° Video and Caching Implications

Niklas Carlsson, Derek Eager

Abstract—The demand and usage of 360° video services are expected to increase. However, despite these services being highly bandwidth intensive, not much is known about the potential value that basic bandwidth saving techniques such as server or edge-network on-demand caching (e.g., in a CDN) could have when used for delivery of such services. This problem is both important and complicated as client-side solutions have been developed that split the full 360° view into multiple tiles, and adapt the quality of the downloaded tiles based on the user's expected viewing direction and bandwidth conditions. To better understand the potential bandwidth savings that caching-based techniques may offer for this context, this paper presents the first characterization of the similarities in the viewing directions of users watching the same 360° video, the overlap in viewports of these users (the area of the full 360° view they actually see), and the potential cache hit rates for different video categories, network conditions, and accuracy levels in the prediction of future viewing direction when prefetching. The results provide substantial insight into the conditions under which overlap can be considerable and caching effective, and can inform the design of new caching system policies tailored for 360° video.

Index Terms—360° streaming, caching, viewport overlap

I. INTRODUCTION

Interactive streaming [1]–[7] such as 360° video put the users in control of their viewing direction and have the opportunity to revolutionize what users expect from their viewing experiences. Already today, popular services such as Facebook and YouTube offer large catalogues of 360° content. With rapidly increasing 360° content catalogues and the introduction of relatively inexpensive user interfaces (ranging from smartphone-based solutions to dedicated head mounted displays), the demand for 360° streaming services can only be expected to increase.

With 360° streaming services being highly bandwidth intensive, identifying and understanding bandwidth saving opportunities in the wide-area delivery of 360° video is therefore becoming an increasingly important problem. Perhaps the most popular bandwidth saving opportunity studied in the research literature is based on the observation that, with 360° video, only a limited fraction of the full view (called the *viewport*) is displayed at each point in time. Motivated by this observation, to reduce the bandwidth usage and to improve the expected playback quality given a fixed bandwidth, different streaming

delivery techniques have been studied that allow alternative playback qualities to be delivered for each candidate viewing direction [1], [2], [8]–[11].

With video delivery systems using HTTP-based Adaptive Streaming (HAS), a video is split into chunks (e.g., 2-5 seconds in duration) that are each encoded at multiple quality levels, allowing clients to adapt their playback quality based on current network conditions, for example, and to build up a buffer to protect against stalls that may be caused by future bandwidth variations. With 360° video, each chunk can further be split into multiple tiles, each corresponding to a portion of the 360° view. This division into tiles complicates prefetching, since now, when prefetching data from a future chunk, the client player needs to determine which tiles from the chunk to prefetch and a quality level for each. The prefetching policy must address a prefetch-aggressiveness tradeoff [7] and balance the use of a larger buffer (to protect against stalls) against making prefetching decisions closer to the time of playback (improving predictions of future viewing directions). To address this problem various head-movement prediction techniques have been proposed and evaluated [8], [12], [13]. However, prior work has not considered the implications of tiling and associated quality-adaptive prefetching techniques for 360° video on the performance of content caches.

Naturally, proxy caches, server-side caches, and other network- and server-side aggregation techniques that try to reduce the amount of data being transferred from disk or over a network are most efficient if there is a significant overlap in the data being requested. To better understand the potential bandwidth savings of caching-based techniques for 360° video delivery, in this paper we characterize the similarities in the viewing directions and viewports (i.e., the area of the full 360° view that each user sees) of users watching the same video, and then analyze and discuss the implications these findings may have on caching performance. To the best of our knowledge, this is the first paper to analyze the viewport overlaps between users watching the same video and the implications that such overlaps have on the caching of tiled 360° video.

The paper has three main parts, with the second and third parts building on the prior parts. First, we present a general analysis of the similarities in viewing direction among different users when at identical playback points within the same 360° video; e.g., as measured by angular differences of the viewing directions, overlap in viewports, and how the viewport's overlap with the aggregate view cover from prior user views increases with the number of such users. This

N. Carlsson is with Linköping University, Sweden.

E-mail: niklas.carlsson@liu.se

D. Eager is with University of Saskatchewan, Canada.

E-mail: eager@cs.usask.ca

analysis provides insight into inherent similarities in viewing behavior, using measures that are not affected by the details of how video data is delivered to users.

Second, we extend the analysis to incorporate chunking of the video content, and the chunk granularity in particular, allowing us to evaluate its impact on the insights in the first part of the paper. This analysis is important with respect to understanding how similarities in viewing direction would impact caching performance. For example, consider the case where two users have significantly different viewing directions at a particular time instant, and yet over the time duration of a chunk have essentially the same viewport cover.

Finally, we present a trace-based analysis in which we simulate a proxy cache and evaluate the cache hit rates observed when using prefetching algorithms that attempt to adaptively select which tiles to download and the quality of each to optimize the user’s quality of experience. The observed cache hit rates reflect not only viewing direction similarities, both at identical time instants (as analyzed in the first part of the paper) and over the time duration of a chunk (as analyzed in the second part of the paper), but also differences in chunk quality selections caused by bandwidth variations and uncertainties in viewing direction prediction.

Throughout our analysis we use head-movement traces collected for different categories of 360° video [7], allowing us to provide quantitative example comparisons and deliver insights into how viewing direction similarities and potential caching performance depend on the nature of the 360° video content. In contrast to most of the 360° video measurements reported in prior work, our traces capture head movements throughout full video playback sessions, and we are therefore able to observe how our results vary as video playback progresses from beginning to end. For evaluation of cache performance, we combine our traces with previously collected network measurements capturing a wide range of network conditions [14], [15].

The results provide substantial insight into the conditions under which overlap can be considerable and caching effective. Particularly noteworthy perhaps are the substantial differences observed between different video categories and, in some cases, playback positions within the video, and the impact of prefetching accuracy on caching effectiveness. For example, the category of videos for which “the main focus of attention is deemed to always be at the same location in the video” [7] appears to provide the greatest opportunities, among the categories we consider. However, this is not the case until 20-30 seconds into these videos, as viewers of these videos often have an initial exploratory phase during which viewing similarities are smaller compared to the category of videos in which the “object of attention is moving across the 360° sphere” or the category in which “the users take a virtual ride in which the camera is moving forward at a high speed”. Caching effectiveness is greatest when the viewing direction predictions used in prefetching are accurate and bandwidth conditions are relatively stable.

Our measurement and analysis results can inform the design of new caching system policies tailored for 360° video. Our results may also have implications for other policies. For

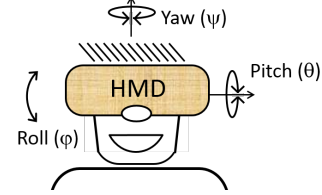


Fig. 1. Head-movement coordinates: Yaw, pitch, and roll.

example, cache hit rate may benefit from cap-based network solutions that stabilize the bandwidth seen by individual clients (e.g., [16]). With respect to prefetching policies, our results show how the value of using the viewing directions of previous users for viewport prediction varies among different 360° video categories and, in some cases, also depends on the playback position.

The remainder of the paper is organized as follows. Section II presents background and introduces the head-movement dataset used here. Section III presents our analysis of viewing direction similarities between pairs of users at identical playback points, pairwise viewport overlaps, and viewport overlaps with aggregate view covers from different numbers of prior users. Section IV extends this analysis to take into account the chunk granularities used, before Section V presents our trace-based simulations of cache performance under different network bandwidth conditions and uncertainties in viewing direction prediction accuracies. Finally, Section VI presents related work and Section VII concludes the paper.

II. BACKGROUND AND DATASET

360° videos capture the view in all directions and allow users to look in any direction at each point during playback; e.g., by moving their head while wearing a head mounted display (HMD). While 360° videos also can be viewed in the browser on PCs, on smartphones, or on tablets, for the work presented here we assume use of an HMD. Figure 1 shows an example user wearing an HMD and defines the viewing angles (i.e., yaw, pitch, and roll) used in our work.

All angles are measured in degrees and normalized so that two users will have the same recorded viewing direction at a given point during their viewing of the same video whenever their viewports completely overlap, regardless of original head positioning. Here, yaw ($\pm 180^\circ$) measures sideways rotations (relative to a 0° line corresponding to the initial viewing direction as set in the video), the pitch ($\pm 90^\circ$) vertical head rotations (relative to a horizontal plane), and the roll ($\pm 90^\circ$) rotations of the head (relative to holding the head straight).

For our analysis we use a dataset collected by Almquist et al. [7]. The dataset consists of fine grained head-movement data collected when 32 people watched 360° videos from a set of 30 such videos. The videos were downloaded and played in 4K resolution, were 1-5 minutes long (3 min. on average), and were (by the authors) split across five categories [7, p. 260]: *exploration* (“no particular object or direction of special interest and the users are expected to explore the entire sphere throughout the video duration”), *static focus* (“the main focus of attention is deemed to always be at the same location in the video”), *moving focus* (“story-driven videos where there is an object of special interest that is moving across the 360°

sphere”), *rides* (“the users take a virtual ride in which the camera is moving forward at a high speed, making users feel that they too are moving forward quickly”), and *miscellaneous* (“includes videos that were deemed to have a mix of the characteristics of the other categories or had a hard-to-classify, unique feel, to them”).

In total, the dataset includes head movements from 439 unique viewings (totaling 21 hrs and 40 min). The “semi-random” design of the user study ensured that all 32 users watched one “representative” video from each category (these videos were named “Zayed Road”, “Christmas scene”, “Christmas story”, “F1”, and “Hockey” in the Almquist et al. paper), while the other videos got between 8-13 views each. In this paper, we primarily focus on the representative videos for the first four (more well-defined) categories, as these allow for a richer head-to-head comparison of the similarities and differences in viewing direction, and hence also of the caching opportunities, when multiple viewers watch the same video, but also report some summary results for the other videos.¹ Since Almquist et al. found that the majority of head movements are yaw movements, followed by pitch, with only small roll movements, we focus only on yaw and pitch.

III. SIMILARITY CHARACTERIZATION

In this section we present an initial characterization of the viewing similarities and differences between users watching the same video. For each video, we calculate and report summary statistics based on the viewing directions observed every 50ms. To account for the timestamps not always aligning perfectly between the traces, we use interpolation and note that good accuracy is ensured by the use of a measurement granularity of 10ms (i.e., 100 measurements per second) in the data collection.

A. Pairwise viewing differences

First, we consider the difference in viewing direction of two users at identical playback points within the same video, as measured by the angle between these directions. Figure 2 shows cumulative distribution functions (CDFs) of the pairwise differences, when combining the differences in both yaw and pitch, for all pairs of viewing sessions of each of the representative videos. (For each of these videos we have 32 user traces and therefore 496 pairs.) In particular, Figure 2(a) shows CDFs for the differences, as measured every 50 ms throughout the viewing sessions, and Figure 2(b) shows CDFs for the average of these differences for each session pair.

As expected, the pairwise differences are substantially larger for the *explore* category than for the other categories (i.e., *static*, *moving*, and *rides*). For example, the close-to-straight *explore* line in Figure 2(a) suggests that the viewing directions of users watching *explore* videos are close to independent. In contrast, for the other categories the view angle differences are less than 45° for 80% of the time instances, showing that viewers of these three video categories often are looking at the same parts of the video.

¹When referring to these videos we will borrow the term “representative” from the original paper to refer to these particular videos.

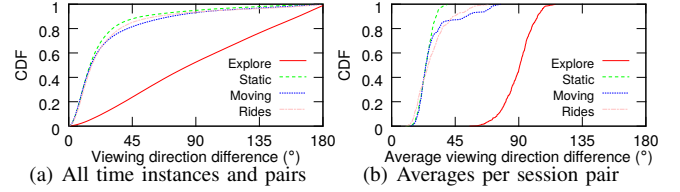


Fig. 2. CDFs of pairwise viewing direction differences; representative videos.

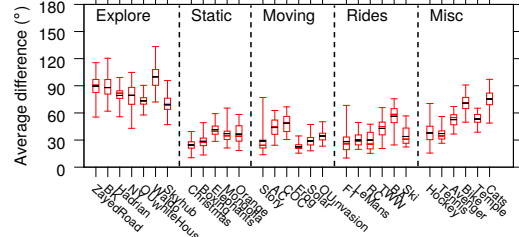


Fig. 3. Pairwise average viewing direction differences for each video.

These significant differences among the categories are also clearly visible when considering the viewing direction difference averaged over the entire playback duration (Figure 2(b)) and when considering the average differences also for the other videos in the dataset (for which there were fewer traces). For example, Figure 3 shows box-and-whisker plots in which we have included results for all videos, broken down per the categorization provided by Almquist et al. [7]. For each video the figure shows the minimum over all pairs of sessions of the average viewing direction difference (bottom marker), 25-percentile (bottom of box), median (middle red marker), 75-percentile (top of box), maximum (top marker), and average (black marker). Again, the pairwise differences are consistently substantially larger for the *explore* category than for the other well-defined categories (i.e., *static*, *moving*, and *rides*). Only a few of the hard-to-classify videos in the *miscellaneous* category see similar pairwise differences.

While the above results are based on the total directional differences across both yaw and pitch, we have found that the observations (and values) are very similar when focusing on the yaw angle only. In general, the head movements are much smaller along pitch, with angular differences (again) most noticeable for the *explore* category. This is illustrated in Figure 4, which breaks down the angular differences observed in Figure 2(a) into yaw ($|\psi_A - \psi_B|$) and pitch ($|\theta_A - \theta_B|$).

B. Pairwise viewport overlap

We next consider the pairwise viewport overlaps. Similarities in what content clients download and what they actually watch depend not only on the users’ viewing directions, but more importantly on their viewports. Here, we consider two types of viewports. First, we consider the 2D area of the viewing field being displayed (i.e., the area of immediate interest to the user). Let $W \times H$ define this area, where W and H are the width and height of the viewport of consideration (as measured in degrees), respectively. Second, motivated by most head movements being along the yaw angle, we consider a *sliced version*, in which we ignore the pitch and only consider the yaw angle. While each user typically would only watch part of such a slice at each time instance, this abstraction better

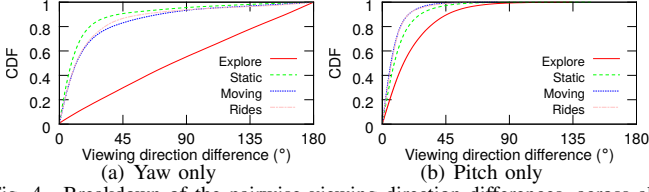


Fig. 4. Breakdown of the pairwise viewing direction differences, across all time instances and user pairs.

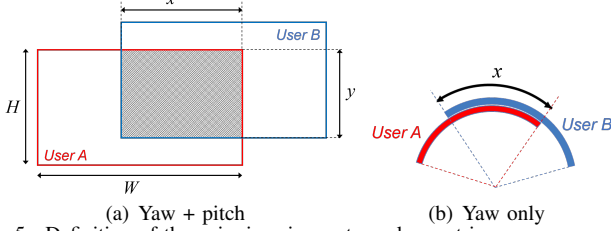


Fig. 5. Definition of the pairwise viewport overlap metric.

matches systems that opt to use vertical tiles (e.g., with higher quality in the range of typical pitch angles and somewhat lower quality downwards and upwards in the viewfield).

Metrics: Consider the viewports of two arbitrary users A and B at the same playback point t of the video. Figure 5(a) shows the viewport overlap when taking into account both the yaw and the pitch angle, whereas in Figure 5(b) we consider the yaw angle alone (this time observing the viewports “from above”). Given the small variations in pitch observed in prior studies, this second metric can be of great interest on its own. In both figures, the viewports of users A and B are shown in red and blue, respectively, and x denotes the overlap along the yaw angle. Furthermore, in Figure 5(a), y denotes the overlap in pitch and the shaded area ($x \times y$) shows the overlap when accounting for both angles. In the following, we report the normalized overlap, equal to $\frac{xy}{WH}$ and x/W , respectively. In our calculations we account for wraparound effects along the yaw angle (using $x = \max(0, W - \min(|\psi_A - \psi_B|, 360 - |\psi_A - \psi_B|))$, where ψ_A and ψ_B are the yaw angles for the two users) but do not consider overlaps due to users catching a glimpse of what is behind them due to pitch angles outside the range ± 90 (using $y = \max(0, H - |\theta_A - \theta_B|)$, where θ_A and θ_B are the pitch angles for the two users).

Results for representative videos: Figure 6 shows CDFs of the normalized pairwise overlap for the representative videos when using a 120×67.5 viewport. Here, Figure 6(a) shows CDFs for the pairwise overlap at identical playback points (as measured every 50 ms) and Figure 6(b) shows CDFs for the average of these overlaps for each session pair. As before we observe significant differences when comparing the *explore* category with the other categories. For example, with the *explore* video, more than 35% of the time there is no pairwise overlap, whereas for the other categories there is at least a 50% overlap in more than 80% of the instances. (See Figure 6(a).) Furthermore, considering the average normalized pairwise viewport overlap (Figure 6(b)), no pair of *explore* sessions had an average overlap of more than 40%, while less than 6.5% of the *moving* session pairs, less than 1% of the *rides* session pairs, and none of the *static* session pairs had an average overlap that did not exceed 40%. In fact, for these three categories, more than 70% of the sessions see an average

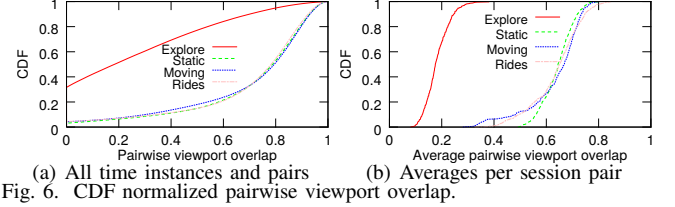


Fig. 6. CDF normalized pairwise viewport overlap.

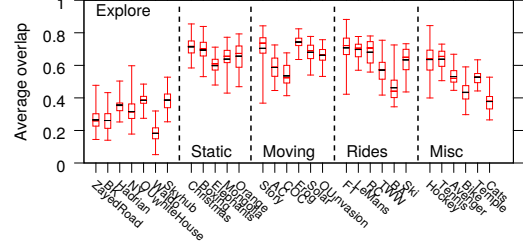


Fig. 7. Average normalized pairwise overlap for all videos. (Viewport size 120×67.5 .)

overlap of at least 60%.

Results for other videos: Similar large differences were observed when calculating the average normalized pairwise overlap for other videos. Figure 7 shows per-video box-and-whisker plots for the average normalized pairwise overlap when considering a 120×67.5 viewport. Although there are significant differences between the videos in each category, these results clearly show that there are substantial overlaps for all videos in the *static*, *moving*, and *rides* categories. The above observations suggest that there may be substantial caching opportunities with these video categories.

Impact of viewport: Figure 8 shows similar summary statistics for the representative videos for five alternative viewports (the last two ignoring differences in pitch). We note that as the viewports become larger, the overlaps increase.

Longitudinal playpoint dependencies: Note that pairwise overlaps vary over the playback duration. For example, all clients start with the same viewing direction and prior work [7] has shown that with *static* videos there is often an initial exploration phase. Figures 9(a) and 9(b) show the overlap averaged over all session pairs as a function of the time from the start of the video, for two example viewports; the first (120×67.5) taking pitch into consideration and the second (90 full) ignoring pitch. In addition to smaller initial average overlaps for the *static* video, resulting from initial exploration, we also observe a somewhat smaller average overlap at the beginning of the videos in the *rides* and *moving* categories than towards the end of those videos. This suggests that there may be opportunities for cache hit rates to improve over the duration of a video session.

C. Viewing sequence analysis

Clearly, the overlap (and also the expected cache hit rate) increases as more users view the same video. To gain further insight into viewport overlaps and implications for potential cache performance, we now look beyond pairwise viewport overlaps and consider overlaps among larger sets of users. Specifically, we evaluate how the viewport overlap with the aggregate view cover from prior user views increases with the number N of such users.

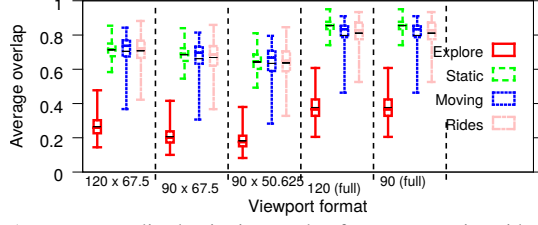


Fig. 8. Average normalized pairwise overlap for representative videos, when using different viewport sizes.

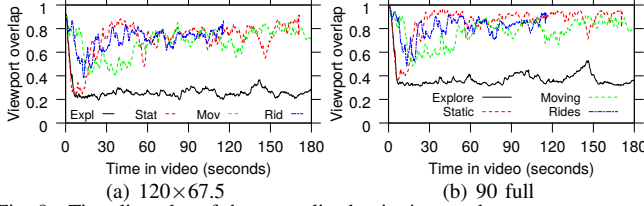


Fig. 9. Time-line plot of the normalized pairwise overlap.

Evaluation method and metrics: For each representative video, we created 1,000 random orderings of the 32 viewing sessions recorded in the dataset for that video, and for each sequence and viewing session, evaluated the overlap at identical playback points between the respective user's viewport and the aggregate viewing area covered by all prior users in that viewing sequence. For this analysis, we ignore pitch (i.e., use vertically sliced viewports) and for each time instance and session sequence, we first merge the viewport coverage of all N prior users into a number of non-overlapping (merged) viewport areas (as represented by the blue rectangles in the example shown in Figure 10(a)). Then, we calculate the overlap of these non-overlapping (merged) viewport intervals with the current user's viewport (overlap represented by the bottom green rectangles in Figure 10(a)), before adding this user's viewport to the merged intervals and repeating the calculations for the next user in the sequence. For these calculations we keep track of a list of non-overlapping intervals that have been merged thus far, and then calculate the sum of the sizes of the intersections of these intervals with the current user's viewport. In general, both the calculations needed to merge intervals and to calculate intersections of intervals require a significant number of cases to consider. Figure 10(b) illustrates the six intersection cases that arise assuming that the most recent viewport goes from $a = 0$ to b , and the (merged) interval from prior user sessions goes from c to d (modulus 360).

Category and viewport dependencies: Figure 11 shows CDFs of the normalized viewport overlap for the representative videos and different numbers of prior users N , where the CDFs are each over all 1,000 random sequences and all playback points at a granularity of 50 ms. Here we used a sliced viewport with width $W = 90$. We note that there is a substantial increase in the normalized overlap as N increases, but with diminishing returns with each doubling of N . Note that as N increases and the CDFs approach the ideal case with all probability mass concentrated at a normalized overlap of 1, the differences between the results for the representative videos diminish. In fact, for $N = 16$ and a larger viewport of $W = 120$, the distribution of the normalized overlap with the *explore* video (Figure 12(b)) has greater mass on larger values

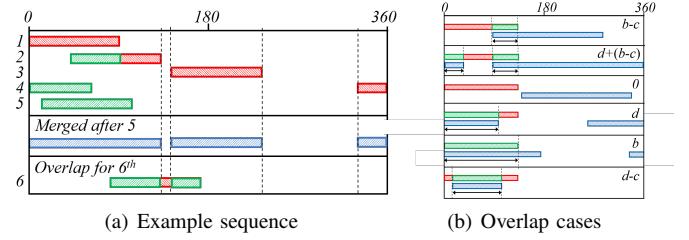


Fig. 10. Examples illustrating the combined multi-user viewport coverage and a user's overlap with prior users.

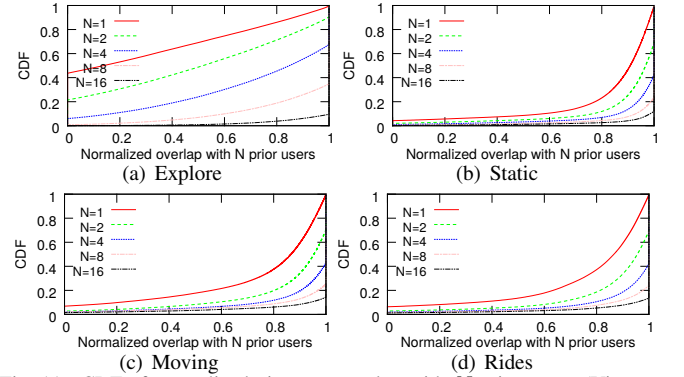


Fig. 11. CDF of normalized viewport overlap with N prior users. (Viewport size $W=90$.)

than that for the other representative videos (as exemplified by the *static* video in Figure 12(d)). More generally, differences between categories, as seen in the results of Figure 12, are larger for smaller viewport sizes and for smaller N .

Longitudinal evaluation: The above observations also hold when considering the normalized overlap observed over time. Figures 13 and 14 show the corresponding timeline plots of the average (over the 1,000 random orderings of viewing sessions) normalized viewport overlap. Note that the benefits of more prior video viewings increase when there is more variability in where users are looking (e.g., *explore* videos or the beginning of the *static* video). Interestingly, the improvements are even larger for median overlap, as seen in Figure 15. The larger median improvements show that the majority of the sessions quickly see significant benefits from each additional prior client, but that there are a few outliers (that impact the averages) which often require more prior clients before seeing the same benefits. For example, with just four prior clients, in the case of the *static* video, the majority of clients have 100% overlap from roughly the 15 second mark.

IV. CHUNK GRANULARITY ANALYSIS

It is important to remember that caching (and video delivery itself) typically is done on a per-chunk basis. The viewport may change during the playback duration of a chunk, resulting in a larger per-chunk viewport cover than the viewport at an individual playback point. The overlaps between per-chunk viewport covers and those of prior clients are important in caching. We next study and report on per-chunk statistics such as the angular changes in viewing direction during the playback duration of a chunk, and per-chunk viewport cover sizes and overlaps.

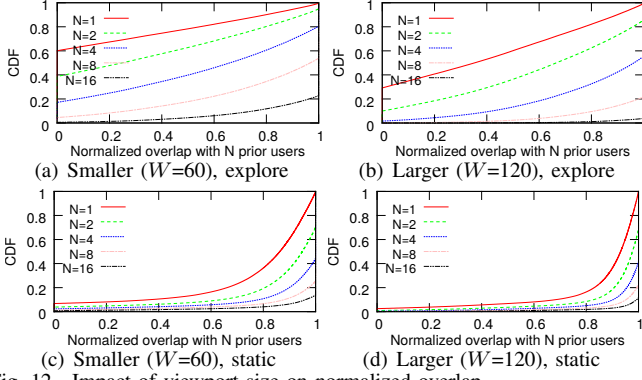


Fig. 12. Impact of viewport size on normalized overlap.

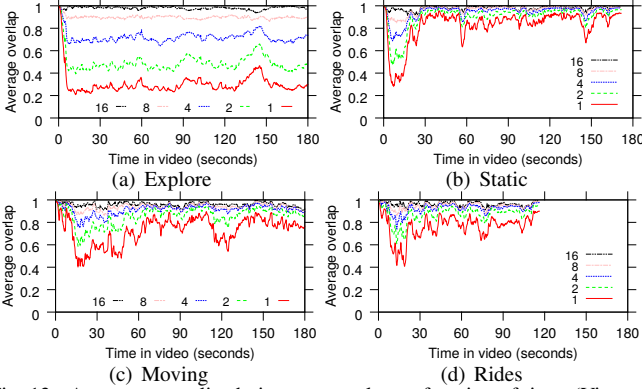


Fig. 13. Average normalized viewport overlap as function of time. (Viewport size $W = 90$.)

A. Changes in viewing direction

Figure 16 illustrates how the total viewing field covered during the playback period of a chunk, and the maximum changes in viewing direction during this time period, are determined from the fine-grained head movement data in our dataset. Here, t_0 denotes the time at which the chunk starts playback, and τ its duration. For this time period, the small head movements that were captured at a 10ms granularity in the trace data are used to calculate the maximum accumulated changes to the left (i.e., ψ^-), to the right (i.e., ψ^+), upwards (i.e., θ^+), and downwards (i.e., θ^-), relative to the original viewing direction (ψ_0, θ_0) at time t_0 . Using fine-grained measurements allows us to keep track of wraparound effects and ensures accurate calculation of these values.

Impact of chunk granularity: Figure 17 shows CDFs of the bound on the maximum viewing direction change given by $\sqrt{(\psi^+ + \psi^-)^2 + (\theta^+ + \theta^-)^2}$ for the representative videos and a range of chunk durations, from very small (200ms) to very large (10s). As before, the *explore* category stands out, with much larger head movements. However, note that for intermediate chunk durations (e.g., 2s), the head movements still only cover a small fraction of the view field. For example, for the representative videos the maximum viewing direction changes for 80% of the chunks are upper bounded (as per the above formula) by 57.7°, 34.5°, 36.3°, and 38.7°, respectively. When considering only the yaw angle, the corresponding 80% values are: 51.5°, 25.3°, 31.3°, 34.5°. Figure 18 presents a direct comparison of the CDFs when using both yaw and pitch (as in Figure 17) and when using only yaw, for the case of

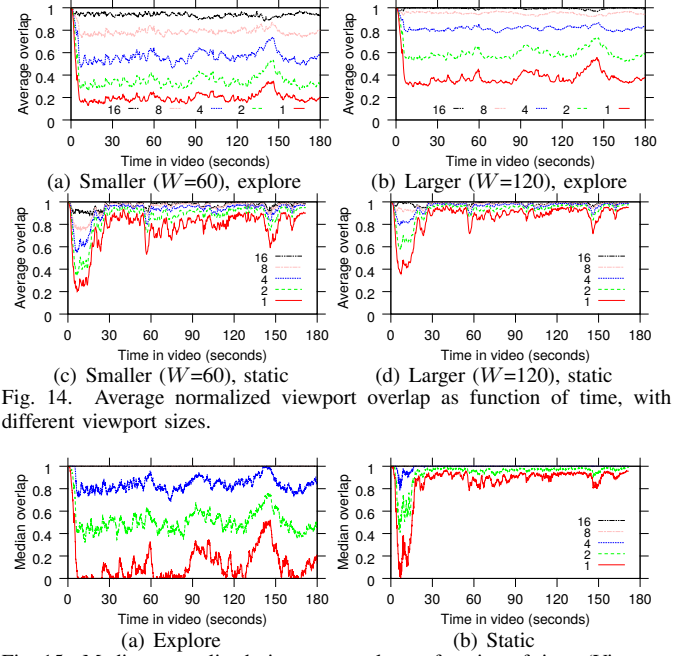


Fig. 14. Average normalized viewport overlap as function of time, with different viewport sizes.

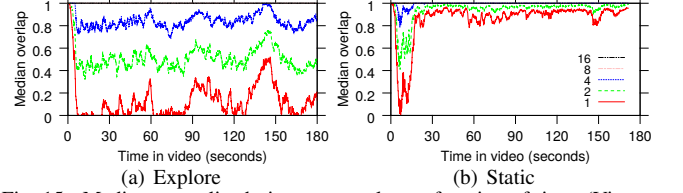


Fig. 15. Median normalized viewport overlap as function of time. (Viewport size $W = 90$.)

2s chunks. As can be seen, the results are similar in nature regardless of whether only the maximum yaw change is used or the bounding angle (across both directions) is used.

B. Per-chunk viewport cover

Metric: To measure the total viewing area that is included within a user's viewport for at least some portion of a chunk's playback period, we calculate a bounding box of the head movements during this time period using the maximum changes in each direction (i.e., ψ^- , ψ^+ , θ^- , θ^+). We define this bounding box as the *per-chunk viewport cover*, with size given by: $\max[360, W + \psi^- + \psi^+] \times \max[180, H + \theta^- + \theta^+]$. Finally, we calculate the normalized per-chunk viewport cover size by dividing by $W \times H$. For the sliced viewport (ignoring pitch), the calculation reduces to simply $\frac{1}{W} \max[360, W + \psi^- + \psi^+]$.

Results for representative videos: Figure 19 presents CDFs of the normalized per-chunk viewport cover size for each of the four representative videos, for four different viewport sizes, and 2 second chunks. When interpreting these results, note that the maximum theoretic normalized cover sizes with these viewport sizes are 8, 14.2, 3, and 4, respectively. While we do see a few extreme values close to the theoretic maximums for the two sliced viewports (120 full and 90 full), the coverage is typically much smaller. For example, with the sliced 90 full (with a theoretic maximum of 4), 80% of the chunks have a normalized cover size of at most 1.57, 1.28, 1.35, and 1.38, respectively, for the four representative videos. These small cover sizes suggest that tiles could fruitfully be prioritized on a per-chunk basis since a significant portion of the potential viewing area is not viewed during the playback of a chunk.

Results for other videos: The above observations are relatively consistent across the videos in each category. Figure 20 shows example distribution statistics for the normalized

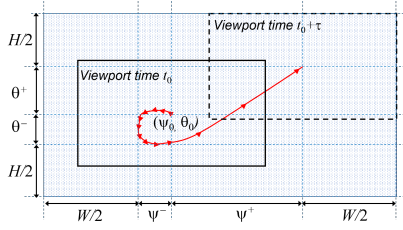


Fig. 16. Bounding the maximum change in viewing direction and the relative viewing field covered by the viewport.

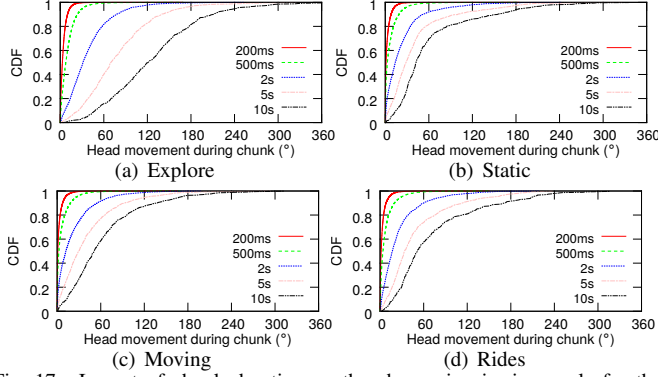


Fig. 17. Impact of chunk duration on the change in viewing angle for the representative videos.

per-chunk viewport cover size for each video when using a 120×67.5 viewport (for which the maximum theoretic normalized cover size is 8). To improve readability, we omit whiskers for minimum (always 1) and maximum (larger than 3.5 for all videos except 3 *static* videos, 1 *moving* video, and 2 *ride* videos). While the relative differences between the video categories in these results (e.g., looking at averages or medians) are less apparent than when looking at the pairwise differences in viewing directions (e.g., Figures 3 and 7), we typically see the largest head movements associated with videos in the *explore* and *miscellaneous* categories and the smallest in the *static* category (even when taking into account that these videos often have an initial exploration phase). Furthermore, we note that the normalized per-chunk viewport cover size is less than two (i.e., less than double the viewport size) for more than 75% of the chunks for almost all videos; Waldo (*explore*) and COC (*moving*) being the two exceptions.

Chunk duration and viewport dependencies: Of course, the cover size depends on both the viewport of consideration and the chunk durations. Figures 21 and 22 show the impact of these two factors on the normalized per-chunk viewport cover size for the representative videos. For example, focusing on the 75-percentile values, except for the three cases of (i) *explore* using a small viewport of 90×50.625 , (ii) *explore* using a chunk duration of 5 or more seconds, and (iii) extremely long duration chunks of 10 seconds, the normalized per-chunk viewport cover size is again consistently below 2. In general, for the *static*, *moving*, and *rides* videos the head movements are substantially smaller, suggesting that prioritizing of tiles may be most suitable for these categories.

C. Pairwise cover overlap

Metric: Naturally, when it comes to resource savings (e.g., by caching or server-side optimization), both viewport over-

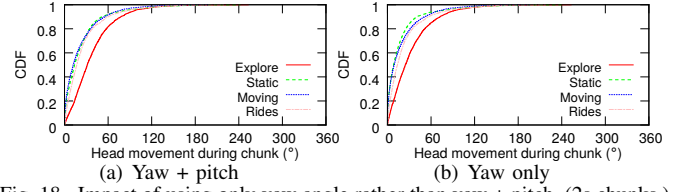


Fig. 18. Impact of using only yaw angle rather than yaw + pitch. (2s chunks.)

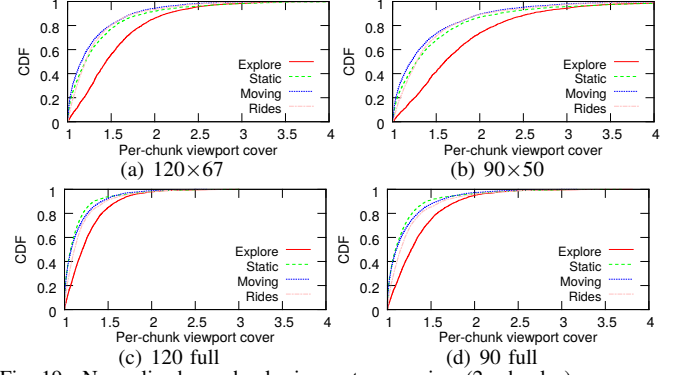


Fig. 19. Normalized per-chunk viewport cover size. (2s chunks.)

laps and chunk boundaries must be taken into consideration. Therefore, we next combine our techniques for analysis of pairwise viewport overlap and for determining per-chunk viewport covers, to measure the pairwise overlap in per-chunk viewport cover. Figure 23 illustrates how this metric is calculated for two users A and B for a particular chunk. Here, we have assumed that user A has the per-chunk viewport cover illustrated by the red box, and user B's corresponding viewport cover is given by the blue box; both bounding boxes calculated as described in the previous section. To calculate the overlap xy when taking into account both dimensions (Figure 23(a)) or x when taking into account only the yaw angle (Figure 23(b)), we extend the methodology used for calculating overlapping viewports to account for the two bounding boxes (capturing the individual viewport cover during the playback duration of the chunk) to be of different size. A case-based analysis is used for this extension (similar to as illustrated for the yaw-only case in Figure 10).

Results for representative videos and example viewports:

Figure 24 shows the pairwise overlap in per-chunk viewport cover taking into account both dimensions. The first two sub-figures show this metric normalized relative to the size of the user's bounding box (i.e., $\frac{xy}{(W+\psi^++\psi^-)(H+\theta^++\theta^-)}$) and relative to the viewport size (i.e., $\frac{xy}{WH}$), respectively, when using a 120×67.5 viewport, and the third sub-figure shows summary statistics (of the first kind) also for other viewports. We note that the *explore* category stands out even more than we have seen before, when considering the overlap normalized relative to the bounding box size (Figures 24(a) and 24(c)). For example, referring to Figure 24(a), while there is at least a 60% overlap in cover for 79-83% of the chunks for the *static*, *moving*, and *rides* videos (83%, 79%, and 83%, respectively), the corresponding fraction of chunks is only 23% for the *explore* video. This reflects the fact that the videos in the *explore* category typically have both larger head movements during a chunk duration, and larger pairwise

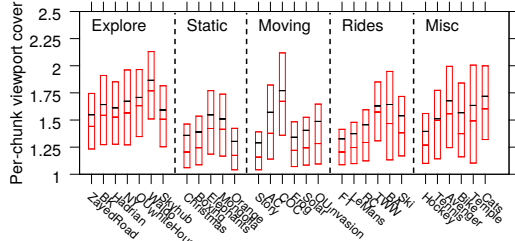


Fig. 20. Normalized per-chunk viewport cover size for each video when using a 120×67.5 viewport. (2s chunks.)

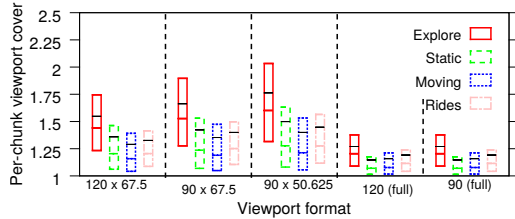


Fig. 21. Impact of viewport format on the normalized per-chunk viewport cover size. (Chunk duration of 2s.)

viewing direction differences (including during the chunk playback period). Furthermore, due to the generally larger head movements associated with *explore*, the variations in the absolute overlap (e.g., as normalized relative to the viewport size, as in Figure 24(b)) is much greater for the *explore* video, and conversely, the variations are smallest for the *static* video.

D. Request sequence analysis

Similar to the prior sub-section, we next extend our analysis of the overlap with the aggregate view cover from N prior user viewings of the same video to account for chunk boundaries. Throughout this section we use 2 second chunks, a sliced 90° viewport, and normalize the reported cover overlap relative to the size of the cover of the user of consideration. In general, the distribution statistics of the overlap between the current user’s per-chunk cover and prior users’ cover for the same chunk (Figure 25(a)) are similar to the corresponding statistics for individual playback points (Figure 11). However, we have observed that the larger head movements and bigger differences in viewing directions associated with the *explore* video result in even greater gains in overlap as the number of prior users increases. In fact, with 16 prior user viewings the overlap is greater than 99% (of the user’s cover) for 94.7% of the chunks for the *explore* video, compared to 88.8%, 86.0%, and 88.5% for the other videos. These observations are also apparent when considering the overlaps seen across the playback durations of the example videos (Figure 26). In fact, during the first 120 seconds of the *explore* video and the initial explore phase of the *static* video the average overlaps when there are $N=8$ and $N=16$ prior users are close to one. In general, however, the overlaps when there are fewer prior users (e.g., $N=1$, $N=2$, and $N=4$ curves) are greater when users are less exploratory (e.g., with *moving*, *rides*, and after the initial exploratory phase of the *static* video). These chunk-level results again highlight important differences in the caching opportunities that different video categories present, and that videos of some categories (e.g., *static*) may require different

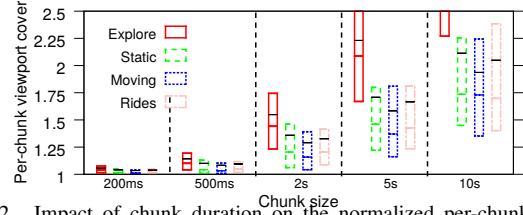


Fig. 22. Impact of chunk duration on the normalized per-chunk viewport cover size. (Viewport size 120×67.5 .)

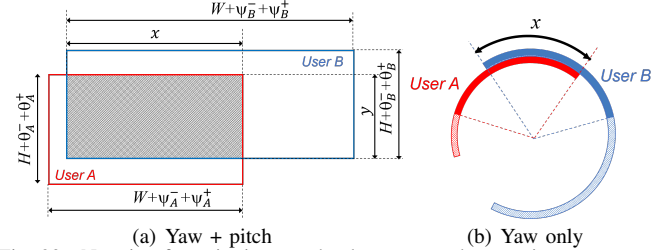
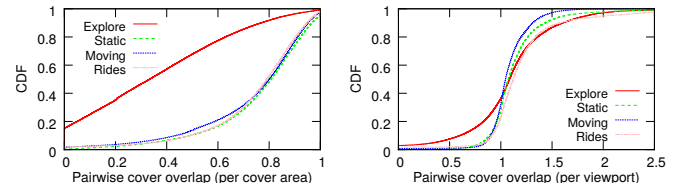


Fig. 23. Notation for pairwise per-chunk cover overlap metrics.



(a) Relative to bounding box (120×67.5) (b) Relative to viewport (120×67.5)

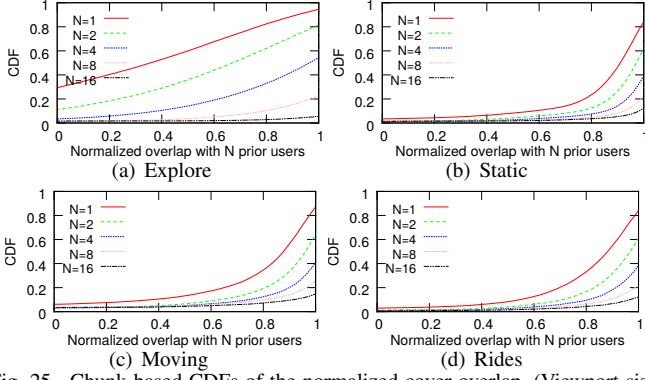


Fig. 25. Chunk-based CDFs of the normalized cover overlap. (Viewport size $W = 90$.)

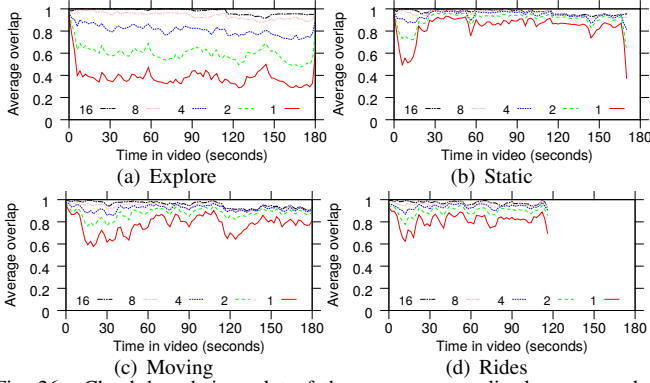


Fig. 26. Chunk-based time plot of the average normalized cover overlap. (Viewport size $W = 90$.)

require some tile selections to be made closer to or further away from the playback time of each chunk, increasing the variability in prediction accuracy also across time.

A. Simulation model

To better understand the impact that download speed variability (caused by the first two uncertainties) and the view direction prediction accuracy have on the cache efficiency under different quality selection algorithms, we use a simple simulation model where we use random functions to capture each of the uncertainties.

To account for the first two uncertainties we build a model based on the following assumptions. For each chunk k , we assume that client player i makes its tile selection based on a quality of experience (QoE) optimization problem taking into account (i) the capacity $C_{i,k}$ drawn from a distribution $P_C(C)$, and (ii) the probability $P_n(n)$ that a specific tile n will be viewed. In particular, each client greedily maximizes the objective function proposed by Almquist et al. [7]:

$$(1 - \beta) \sum_{n=0}^{N-1} P_n(n) u(q_n) - \beta \sum_{n=0}^{N-1} \frac{P_n(n) + P_n(n+1)}{2} |u(q_n) - u(q_{n+1})|, \quad (1)$$

where β is a weight factor giving more (or less) weight to the importance of small quality differences between neighboring tiles in the 360-space versus high expected viewing quality,

and $u(q_n)$ is a concave utility achieved when viewing at quality q_n . At each step of the simulation, each client maximizes this objective function given the capacity constraint that

$$\sum_{n=0}^{N-1} r(q_n) \leq C_{i,k}, \quad (2)$$

where $r(q_n)$ is the size of tile n . To find the optimal solution for a given $C_{i,k}$ and $P_n(n)$ we solve the above optimization problem using dynamic programming [7].

Finally, to account for the third uncertainty, the predicted viewing direction used when solving the above optimization is offset from the actual viewing direction at playback time by an angle $\psi_{i,k}^\epsilon$ chosen by sampling from a probability distribution $P_\psi(\psi)$.

To obtain a hit rate estimate for a particular video and number of previous clients, we average results from 1,000 simulations, each with 32 randomly-ordered users sequentially viewing the video. Each client uses the user head movements recorded in our trace dataset for that user when viewing the respective video. For each chunk prefetch request within each viewing, we (i) draw a random capacity $C_{i,k}$ from the distribution $P_C(C)$, (ii) draw a random offset $\psi_{i,k}^\epsilon$ from the distribution $P_\psi(\psi)$, (iii) use the actual viewing direction $\psi_{i,k}$ that the user has at the start of the playback of the chunk and $\psi_{i,k}^\epsilon$ to determine the center tile used for the optimization, (iv) solve the above optimization problem using the $C_{i,k}$ and the distribution $P_n(n)$ (rotated by $\psi_{i,k} + \psi_{i,k}^\epsilon$), and (v) download the qualities of tiles for the chunk that are determined by the optimization. To emulate the behavior of a cache, we keep track of prior client requests for tiles of the same chunk. For our simulation we assume that the system always starts with an empty cache and measure how the hit rate (both in terms of tile objects and bytes delivered) changes as more and more users view the same video.

We do not model individual clients buffer conditions, correlations in the chunk qualities that individual clients may request for back-to-back chunks, or the correlations between the bandwidths that clients may observe during download of consecutive chunks. While these aspects may help model the quality of experience and performance of individual clients, they are not needed to capture the performance of a network or server-side cache.

B. Parameters and example distributions

Bandwidth variations: For the distribution $P_C(C)$ we use two distributions obtained by drawing random samples from two real-world datasets, and two synthetic distributions. The real-world datasets are: (i) 10,000 download bandwidth measurements collected by mobile 3G and 4G users of a dominant national speed testing service [15] over a 19 hour window on Feb. 15-16, 2015, and (ii) 10,000 sample points from “bus” commuter traces collected in Norway by Riiser et al. [14] between Aug. 28, 2010, and Jan. 31, 2011. The synthetic distributions we use are: (i) a distribution in which the bandwidth capacity C varies across three different levels such that C is equal to the average bandwidth 40% of the time, twice the average bandwidth 20% of the time, and half

TABLE I
HEAD MOVEMENT VARIATIONS, AS MEASURED BY YAW ANGLE CHANGE,
OVER A T SECOND INTERVAL ($T = 2, 5$, OR 10 SECONDS).

Category	Standard deviation		
	2 seconds	5 seconds	10 seconds
Explore	50.77°	79.85°	94.09°
Static	35.94°	46.32°	46.93°
Moving	35.77°	48.10°	57.42°
Rides	38.94°	50.02°	52.44°

the average bandwidth 40% of the time, and (ii) a constant bandwidth capacity. To account for the fact that bandwidths have increased substantially since the traces in the real-world datasets were collected (2010-2011 and 2015, respectively) and to ensure a more fair head-to-head comparison across the different distributions, we scale the bandwidths in the real-world datasets and choose parameters for the synthetic distributions so that the average bandwidth in each case is the same. Furthermore, we use normalized units so that a normalized bandwidth of 1 corresponds to the bandwidth needed to deliver all tiles at the maximum quality.

Head movements, their prediction uncertainties, and optimized quality selection: To determine choices for the $P_\psi(\psi)$ and $P_n(n)$ distributions, we considered the yaw angle changes in the traces from the head-movement dataset over different time intervals and for different video categories. With the averages close to zero and the CDFs following s-shaped distributions [7], we decided to approximate yaw angle change distributions using normal distributions and used these (or variations) for the uncertainty $P_\psi(\psi)$ in yaw prediction and the uncertainty in head movements $P_n(n)$ used for the optimizations. Table I reports the standard deviations observed for each video category and three different time intervals $T = 2, 5, 10$. Clearly, the best $P_\psi(\psi)$ distribution to use here would depend on the prediction techniques being used and there can be both better and worse predictors of future head movements than simply using the current viewing direction (as implicitly assumed here). For this reason, we apply a scaling factor f_ψ on these measured standard deviations, with a factor f_ψ smaller (greater) than one capturing a more (less) accurate prediction of the future viewing direction. Similarly, we use a factor f_n to scale the standard deviation used for the quality selection optimization distribution $P_n(n)$, with a factor f_n smaller (greater) than one capturing a more (less) concentrated distribution. As our default values we use the 10 second values of each category with $f_\psi = f_n = 1$.

Finally, for the example simulation results presented here, we consider a sliced 360° video with each 2-second chunk split into 6 tiles, each covering 60 degrees, and for which the tile encoding rates are each proportional to one of seven quality levels (found in an example YouTube video): 0, 144, 268, 625, 1124, 2217, 4198 (in normalized units). For the dynamic programming optimization, we use these integers as the corresponding tile sizes together with a default average bandwidth C of 12,000, resulting in a normalized average bandwidth of $12000 / (4198 \times 6) = 0.476$ (allowing benefits from quality-adaptive tile delivery similar to those in prior works [1], [8], [17]). For the utility function we extend the large-screen model by Vleeschauwer et al. [18] to include a

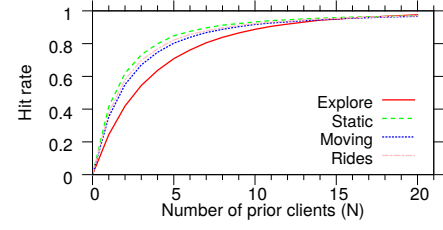


Fig. 27. Object hit rate for trace-based simulations with fixed bandwidth.

“black-out penalty” associated with a missing tile:

$$u(q) = \begin{cases} b \cdot \frac{(q/\theta)^{1-a}-1}{1-a}, & \text{if } q = 144, 268, 625, 1124, 2217, 4198 \\ -u(4198), & \text{if } q = 0 \end{cases} \quad (3)$$

where a , b , and θ are screen dependent parameters with values chosen as 2, 10, and 200, respectively, to match their large-screen model, and the negative utility when $q = 0$ captures the black-out penalty associated with missing tiles.

C. Example results

In this section we focus on the hit rate as a function of the number of prior users that have watched the same video. Each result for a particular video and scenario is an average from 1,000 simulations, each using a random ordering of the 32 user sessions for that video from our trace dataset.

Results for representative videos: Figure 27 shows a baseline comparison of the tile object hit rates for the representative videos, using the 10 second values from Table I and $f_\psi = f_n = 1$. This figure clearly illustrates that better cache performance is achieved with the *static*, *rides* and *moving* videos compared to with the *explore* video. This observation is not surprising given the results reported in previous sections, and is also consistently seen with other distribution and parameter settings. For example, with four prior clients (i.e., $N = 4$), the object hit rate for the *static*, *rides*, and *moving* videos ranges between 0.75-0.80, while for the *explore* video it is only 0.64. These differences would have a large impact on bandwidth requirements. Note for example that with $N = 4$, the object miss rate for *explore* is 80% higher (a factor of 0.36/0.20) than for the *static* video. In the remainder of this section we present results only for the two extreme cases of *static* and *explore* videos, but note that the results for *rides* and *moving* are relatively similar to those of *static*.

Object vs byte hit rates: For our default settings, we have observed higher byte hit rates than object hit rates (Figure 28). For example, with four prior clients, the byte hit rates for the four representative videos range from 0.73-0.85, substantially higher than the object hit rates.

Impact of client’s bandwidth variability: We have observed that hit rates typically reduce the greater the bandwidth variability (Figure 29). For example, for $N=4$, the object hit rates for the *static* video are 0.60 with the national speed test service, 0.61 with the Norwegian bus traces, 0.66 with the three-level distribution, and 0.80 when the bandwidth is constant. Note however that the relative impact of bandwidth variability is smaller for the *explore* video than the *static* video, showing that higher uncertainty in viewing direction

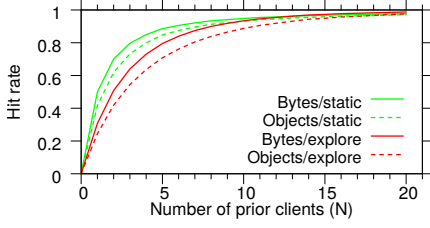


Fig. 28. Object hit rate vs byte hit rate for trace-based simulations with fixed bandwidth.

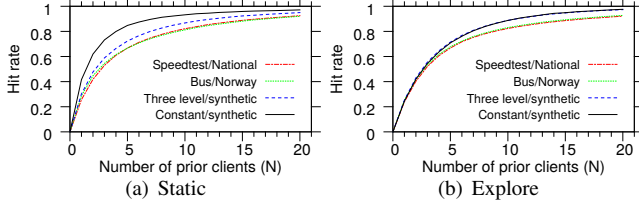


Fig. 29. Object hit rate for trace-based simulations using different network bandwidth profiles.

and bandwidth do not contribute independently to reduced hit rates.

In the following we show additional object hit rate results for the two extreme cases for bandwidth variation across clients of (a) constant bandwidth (identical for all clients) and (b) the bandwidth distribution obtained by drawing random samples from measurements collected by mobile 3G and 4G users of a dominant national speed testing service [15]. When interpreting these results, it is important to note that clients sharing an edge-cache (e.g., operated by a CDN or in cooperation with a CDN) might be expected to experience more similar bandwidth conditions than in the speed testing data. Also, with the introduction of cap-based solutions [16], and other streaming-aware network solutions, used by different operators to stabilize HAS performance, improve QoE, and to reduce unnecessary bandwidth usage, it seems likely that many networks in the future will provide fairly stable conditions for their streaming clients. Therefore, we believe that likely bandwidth variations fall between these two extremes.

Impact of head movement uncertainties and prediction accuracy: Figures 30 and 31 show results capturing the impact of the prediction accuracy (varying f_ψ ; Figure 30) and the concentration of the $P_n(n)$ distribution used for the utility optimization (varying f_n ; Figure 31). In these figures we use solid lines for the *static* video and dotted lines for the *explore* video. Note that the differences between the two video categories are largest for the constant bandwidth case (or, more generally, are larger when the bandwidth variations are smaller). Although the differences also appear larger for smaller N , it is also necessary to consider the corresponding miss rates as these determine the bandwidth costs. For example, for $N = 4$ and constant bandwidth (Figures 30(a) and 31(a)) there are substantial regions where the miss rates (and hence bandwidth usage) are almost twice as large for the *explore* video as for the *static* video.

Figures 30 and 31 clearly show that the hit rates for small N are much lower when the prediction accuracy is poor and the estimated uncertainty is large, respectively, but that the hit

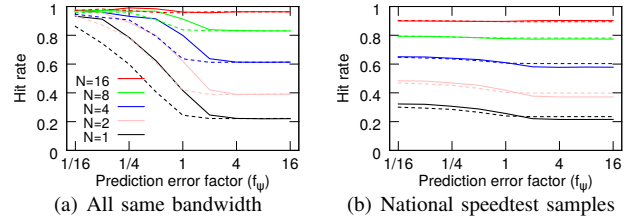


Fig. 30. Impact of the prediction error factor f_ψ used to simulate the error in viewing direction, for the two video categories: *static* (solid lines) and *explore* (dotted lines).

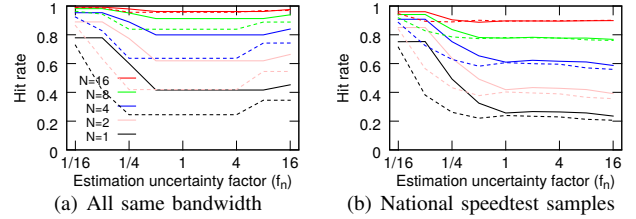


Fig. 31. Impact of the estimated uncertainty factor f_n used in optimization, for the two video categories: *static* (solid lines) and *explore* (dotted lines).

rates go up substantially as N increases also for these cases. These gains are especially visible when all clients have the same bandwidth, illustrating that caching of HAS video (and in this case tiled 360° video) is most efficient when clients have similar bandwidth conditions and request chunks (or tiles) of similar quality. For example, when $f_\psi = 2$, while the first *static* client seeing a non-empty cache (i.e., $N = 1$) has a hit rate below 0.25, the hit rate quickly goes up to 0.61 when N increases to 4, a similar hit rate as for $N = 1$ and $f_\psi = 0.5$.

Impact of average bandwidth: Figure 32 shows that our default case of a normalized bandwidth of 0.476 results in close to the worst-case hit rates, suggesting that the hit rates with tiled 360° video could be greater than suggested by Figures 27-31. Also, when comparing Figures 32(a) and 32(b) it should be noted that owing to our choice of normalized units for bandwidth, the hit rate is always one when all clients have the same (constant) bandwidth above one (Figure 32(a)), whereas bandwidth variations in the national speedtest dataset result in significant periods of bandwidth below one even for average values substantially larger than one. Again, in practice, we expect clients sharing the same cache to see hit rates between the two extremes considered here, with operators likely to strive towards providing increasingly stable network conditions for streaming clients [16].

VI. RELATED WORK

Broadly, the related work can be split into works that consider the head movements during viewing of 360° videos, client-side techniques to provide the best possible QoE (e.g., through adaptive prefetching based on expected viewing directions), and caching of HAS videos. To the best of our knowledge we provide the first study that considers the intersection of these three aspects.

Head-movement characterization: A number of recent works have collected datasets and characterized the 360° viewer behavior [7], [8], [11], [17], [19]–[21]. However, most

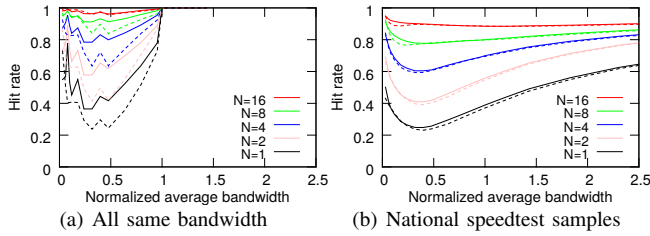


Fig. 32. Impact of the normalized average bandwidth, for the two video categories: *static* (solid lines) and *explore* (dotted lines).

of these datasets use relatively short video segments and do not capture changes in behavior over time or across classes of videos. The primary exception, and the work most closely related to ours, is the work by Almquist et al. [7], as we use their dataset. In their work, they present a category-based characterization of the head movements over time, and analyze how changes in viewing behavior depend on the time window considered, but do not consider overlapping viewports of users watching the same video or other similarity metrics of users' viewing directions.

Client-side techniques: Motivated by HMDs allowing different projection and quality adaptive download techniques [22], recent works have proposed various techniques to adaptively download different qualities for different viewing directions [1], [2], [8], [9], [17], [23]. These techniques typically combine user head movement tracking/prediction [8], [12], [13], [17] and bandwidth management [1], [24]. For example, Bao et al. [8] propose a motion-prediction-based transmission scheme based on viewing behavior data and show that view-dependent 360° transmission schemes with motion prediction can reduce bandwidth consumption by 45% at the cost of only very small performance degradation. Similarly, Hosseini and Swaminathan [1] present an adaptive tile-based streaming solution and show that large bandwidth savings (72%) can be achieved with only small quality degradation. Similarly, Graf et al. [25] studied the impact of projection techniques, quantization parameters, and tile patterns on the playback experience and resource requirements. Others have considered tradeoffs that try to address variations and uncertainties in both the user's bandwidth and viewing direction simultaneously [7], [17], [26]. For example, Sun et al. [26] use simulations and experiments that capture the bandwidth variations, Qian et al. [17] have implemented and tested a tile-based solution on a real network, whereas Almquist et al. [7] note that HAS clients typically try to maintain a steady buffer (to protect against stalls) and consider the optimized prefetch-aggressiveness tradeoff of such clients. In this paper, we leverage the optimization framework provided by Almquist et al. [7] to evaluate the impact prefetching optimizations have on the caching performance of tiled 360° video.

Tile-based spatial video segmentation has been used in several other applications, including to support pan/tilt/zoom interactions during live streaming of high resolution videos [27], for interactive panoramic video [5], interactive 4k video [28], and to allow users to navigate freely through high resolution video feeds while minimizing bandwidth usage [29]. Other prior works have demonstrated interactive tiled streaming

of ultra-high resolution videos based on a user's region-of-interest [30], [31] and crowd-driven prefetch prediction [32].

An alternative to tile-based streaming is to create different versions for each potential viewing direction and let the viewer adapt the version downloaded for each chunk. For example, Kuzyakov and Pio [33] create different smaller-sized versions in which each version has a specific area in high quality and with gradually decreasing quality away from this area. While some of the observations in this paper are applicable to this context, we do not explicitly consider such techniques here.

Bandwidth-interactivity tradeoffs: The tradeoffs between bandwidth constraints, playback quality, and interactivity have also been considered in other contexts. For example, Ma et al. [3] consider these tradeoffs in the context of interactive multiview streaming. HAS also has been leveraged for bandwidth-aware support of other interactive services, including interactive multiview streaming [4], optimized stream bundles [6], and to enhance parts of regular (linear) videos that the users show more interest in [34].

Caching for HAS: Prior works have characterized the caching opportunities for HAS content in mobile networks [35], evaluated the impact that cross traffic has on cache performance [36], identified HAS specific instabilities and other tradeoffs associated with the use of caches combined with HAS [37], [38], and proposed HAS-aware solutions to improve the client performance in such scenarios [37]–[42]. Other works have considered various cache management problems in the context of HAS [43], [44] and optimized replication for interactive multiview streaming [45], [46]. However, none of the above caching papers consider tiled 360° video. In this paper, we present the first characterization and analysis of similarities in head movements between users watching the same video, the users' viewport overlaps, and their implications on caching of tiled 360° videos belonging to different categories.

VII. CONCLUSIONS

This paper uses head-movement traces for different categories of 360° videos, including *explore*, *static*, *moving*, *rides*, to characterize similarities in the viewing directions and viewports of users watching the same video, how these example metrics differ between the different video categories, and to analyze and discuss how such similarities and differences impact the effectiveness of caching tiled 360° videos. To the best of our knowledge, this is the first paper to provide such analysis.

While the use of larger chunk durations and larger viewports slightly reduce some differences observed, our results consistently highlight substantial differences between different video categories in the pairwise viewport overlaps observed and the impact that they have on the potential bandwidth savings of caching-based techniques for this context. For example, with the exception of the initial 20-30 second exploration phase of *static* videos, the *static* videos provide the greatest caching opportunities. However, during this initial phase, their pairwise viewport overlaps are almost as small as for the *explore* videos, which have the smallest overlaps among the

categories considered here. In contrast, *moving* and *rides* videos have a less pronounced exploration phase, and overall often provide similar caching opportunities and performance as the *static* videos. Our results also show that improved viewport prediction techniques [12] may not only help improve user QoE, through the use of more accurate prefetching, but may also help increase cache hit rates (and further reduce bandwidth requirements and improve client performance).

More generally, our results can inform the design of new caching system policies tailored for 360° video, and may also have implications for other contexts than caching. For example, our novel category-based characterization clearly highlights that there are substantial differences among the video categories in the value of using the viewing directions of previous users for viewport prediction. The results also clearly show that cache performance, and hence also likely user QoE, benefit from stable network conditions, motivating the use of cap-based network/server-side solutions or less greedy client-side solutions.

ACKNOWLEDGEMENTS

This work was funded in part by the Swedish Research Council (VR).

REFERENCES

- [1] M. Hosseini and V. Swaminathan, "Adaptive 360 vr video streaming: Divide and conquer," in *Proc. IEEE ISM*, Dec. 2016.
- [2] J. Son, D. Jang, and E.-S. Ryu, "Implementing 360 video tiled streaming system," in *Proc. ACM MMSys*, 2018.
- [3] R. Ma, T. Maugey, and P. Frossard, "Optimized data representation for interactive multiview navigation," *IEEE Trans. on Multimedia*, vol. 20, no. 7, July 2018.
- [4] L. Toni and P. Frossard, "Optimal representations for adaptive streaming in interactive multiview video systems," *IEEE Trans. on Multimedia*, vol. 19, no. 12, Dec. 2017.
- [5] V. R. Gaddam, M. Riegler, R. Eg, C. Griwodz, and P. Halvorsen, "Tiling in interactive panoramic video: Approaches and evaluation," *IEEE Trans. on Multimedia*, vol. 18, no. 9, Sept. 2016.
- [6] N. Carlsson, D. Eager, V. Krishnamoorthi, and T. Polishchuk, "Optimized adaptive streaming of multi-video stream bundles," *IEEE Transactions on Multimedia*, vol. 19, pp. 1637–1653, July 2017.
- [7] M. Almquist, V. Almquist, V. Krishnamoorthi, N. Carlsson, and D. Eager, "The prefetch aggressiveness tradeoff in 360° video streaming," in *Proc. ACM MMSys*, June 2018.
- [8] Y. Bao, H. Wu, T. Zhang, A. Ramli, and X. Liu, "Shooting a moving target: Motion-prediction-based transmission for 360-degree videos," in *Proc. IEEE Big Data*, Dec. 2016.
- [9] J. Son, D. Jang, and E.-S. Ryu, "Implementing motion-constrained tile and viewport extraction for Vr streaming," in *Proc. ACM NOSSDAV*, 2018.
- [10] X. Corbillon, G. Simon, A. Devlic, and J. Chakareski, "Viewport-adaptive navigable 360-degree video delivery," in *Proc. IEEE ICC*, 2017.
- [11] W. Lo, C. Fan, J. Lee, C. Huang, K. Chen, and C. Hsu, "360° video viewing dataset in head-mounted virtual reality," in *Proc. ACM MMSys*, 2017.
- [12] L. Xie, X. Zhang, and Z. Guo, "CLS: A cross-user learning based system for improving QoE in 360-degree video adaptive streaming," in *ACM Multimedia*, 2018.
- [13] F. Qian, L. Ji, B. Han, and V. Gopalakrishnan, "Optimizing 360 video delivery over cellular networks," in *Proc. All Things Cellular Workshop*, Oct. 2016.
- [14] H. Riiser, P. Vigmostad, C. Griwodz, and P. Halvorsen, "Commute path bandwidth traces from 3G networks: Analysis and applications," in *Proc. MMSys*, 2013.
- [15] T. Linder, P. Persson, A. Forsberg, J. Danielsson, and N. Carlsson, "On using crowd-sourced network measurements for performance prediction," in *Proc. IEEE/IFIP WONS*, 2016.
- [16] V. Krishnamoorthi, N. Carlsson, and E. Halepovic, "Slow but steady: Cap-based client-network interaction for improved streaming experience," in *Proc. IEEE/ACM IWQoS*, June 2018.
- [17] F. Qian, B. Han, Q. Xiao, and V. Gopalakrishnan, "Flare: Practical viewport-adaptive 360-degree video streaming for mobile devices," in *Proc. ACM MobiCom*, 2018.
- [18] D. D. Vleeschauwer, H. Viswanathan, A. Beck, S. Benno, G. Li, and R. Miller, "Optimization of http adaptive streaming over mobile cellular networks," in *Proc. IEEE INFOCOM*, 2013.
- [19] X. Corbillon, F. D. Simone, and G. Simon, "360-degree video head movement dataset," in *Proc. ACM MMSys*, 2017.
- [20] S. Fremerey, A. Singla, K. Meseberg, and A. Raake, "AVtrack360: An open dataset and software recording people's head rotations watching 360° videos on an HMD," in *Proc. ACM MMSys*, 2018.
- [21] E. J. David, J. Gutiérrez, A. Coutrot, M. P. Da Silva, and P. L. Callet, "A dataset of head and eye movements for 360° videos," in *Proc. ACM MMSys*, 2018.
- [22] C. Zhou, Z. Li, and Y. Liu, "A measurement study of oculus 360 degree video streaming," in *Proc. ACM MMSys*, 2017.
- [23] C. Zhou, M. Xiao, and Y. Liu, "ClusTile: Toward minimizing bandwidth in 360-degree video streaming," in *Proc. IEEE INFOCOM*, April 2018.
- [24] D. Ochi, Y. Kunita, K. Fujii, A. Kojima, S. Iwaki, and J. Hirose, "HMD viewing spherical video streaming system," in *Proc. ACM Multimedia*, Nov. 2014.
- [25] M. Graf, C. Timmerer, and C. Mueller, "Towards bandwidth efficient adaptive streaming of omnidirectional video over HTTP: Design, implementation, and evaluation," in *Proc. ACM MMSys*, Jun. 2017.
- [26] L. Sun, F. Duanmu, Y. Liu, Y. Wang, Y. Ye, H. Shi, and D. Dai, "Multi-path multi-tier 360-degree video streaming in 5g networks," in *Proc. ACM MMSys*, 2018.
- [27] R. van Brandenburg, O. Niamut, M. Prins, and H. Stokking, "Spatial segmentation for immersive media delivery," in *Proc. ICIN*, 2011.
- [28] J. Redi, L. D'Acunto, and O. Niamut, "Interactive UHDTV at the commonwealth games: An explorative evaluation," in *Proc. ACM TVX*, 2015.
- [29] L. D'Acunto, J. Redi, and O. Niamut, "iCaCoT - interactive camera-based coaching and training," in *Proc. Workshop on Interactive Content Consumption*, 2015.
- [30] A. Mavlanca, P. Baccichet, D. Varodayan, and B. Girod, "Optimal slice size for streaming regions of high resolution video with virtual pan/tilt/zoom functionality," in *Proc. European Signal Processing Conference*, 2007.
- [31] A. Mavlanca, P. Agrawal, D. Pang, S. Halawa, N. Cheung, and B. Girod, "An interactive region-of-interest video streaming system for online lecture viewing," in *Proc. Packet Video Workshop*, 2010.
- [32] D. Pang, S. Halawa, N.-M. Cheung, and B. Girod, "Mobile interactive region-of-interest video streaming with crowd-driven prefetching," in *Proc. IMMPD*, 2011.
- [33] D. Pio and E. Kuzyakov, "Next-generation video encoding techniques for 360 video and VR," Jan. 2016. [Online]. Available: <https://code.facebook.com/posts/1126354007399553/next-generation-video-encoding-techniques-for-360-video-and-vr/>
- [34] G. Gao, H. Zhang, H. Hu, Y. Wen, J. Cai, C. Luo, and W. Zeng, "Optimizing quality of experience for adaptive bitrate streaming via viewer interest inference," *IEEE Trans. on Multimedia*, vol. 20, no. 12, Dec. 2018.
- [35] A. Gouta, D. Hong, A.-M. Kermarrec, and Y. Lelouedec, "HTTP adaptive streaming in mobile networks: Characteristics and caching opportunities," in *Proc. IEEE MASCOTS*, 2013.
- [36] S. Benno, J. O. Esteban, and I. Rimac, "Adaptive streaming: The network HAS to help," *Bell Lab. Tech. J.*, vol. 16, no. 2, pp. 101–114, Sept. 2011.
- [37] V. Krishnamoorthi, N. Carlsson, D. Eager, A. Mahanti, and N. Shah-mehri, "Helping hand or hidden hurdle: Proxy-assisted HTTP-based adaptive streaming performance," in *Proc. IEEE MASCOTS*, 2013.
- [38] D. H. Lee, C. Dovrolis, and A. C. Begen, "Caching in HTTP adaptive streaming: Friend or foe?" in *Proc. ACM NOSSDAV*, 2014.
- [39] E. Thomas, M. van Deventer, T. Stockhammer, A. C. Begen, and J. Famaey, "Enhancing MPEG DASH performance via server and network assistance," *SMPTE Motion Imaging Journal*, vol. 126, pp. 22–27, Jan/Feb. 2017.
- [40] E. Thomas, M. van Deventer, T. Stockhammer, A. C. Begen, M.-L. Champel, and O. Oyman, "Applications and deployments of server and network assisted DASH (SAND)," in *Proc. IBC*, 2016.
- [41] S. K. Mehr, P. Juluri, M. Maddumala, and D. Medhi, "An adaptation aware hybrid client-cache approach for video delivery with dynamic adaptive streaming over HTTP," in *Proc. IEEE/IFIP NOMS*, 2018.

- [42] K. Liang, J. Hao, R. Zimmermann, and D. K. Y. Yau, "Integrated prefetching and caching for adaptive video streaming over HTTP: An online approach," in *Proc. ACM MMSys*, 2015.
- [43] W. Zhang, Y. Wen, Z. Chen, and A. Khisti, "QoE-driven cache management for HTTP adaptive bit rate streaming over wireless networks," *IEEE Trans. on Multimedia*, vol. 15, no. 6, pp. 1431–1445, 2013.
- [44] C. Li, L. Toni, J. Zou, H. Xiong, and P. Frossard, "QoE-driven mobile edge caching placement for adaptive video streaming," *IEEE Trans. on Multimedia*, vol. 20, no. 4, Apr. 2018.
- [45] D. Ren, S.-H. G. Chan, G. Cheung, and P. Frossard, "Coding structure and replication optimization for interactive multiview video streaming," *IEEE Trans. on Multimedia*, vol. 16, no. 7, Nov. 2014.
- [46] L. Toni, G. Cheung, and P. Frossard, "In-network view synthesis for interactive multiview video systems," *IEEE Trans. on Multimedia*, vol. 18, no. 5, May 2016.